«NATIONAL RESEARCH NUCLEAR UNIVERSITY MEPHI»
(Moscow Engineering Physics Institute)

INSTITUTE OF NUCLEAR PHYSICS AND ENGINEERING
DEPARTMENT №40 «ELEMENTARY PARTICLE PHYSICS»

EXPERIMENTAL SEARCH FOR BOSONIC SUPER-WIMP INTERACTIONS

Author _____ D. Kilinkarov

Moscow 2021

TABLE OF CONTENT

INTRODUCTION

There is overwhelming evidence for the presence of dark matter in our universe. Its existence is inferred from a variety of observations, including those of the temperature fluctuations in the cosmic microwave background[1], gravitational lensing [2], mass-to-light ratio in galaxy clusters[3], and galactic rotation curves. In addition, simulations of large-scale structure and galaxy formation require the presence of non-baryonic matter to reproduce the observed cosmic structures [4]. While the microscopic nature of dark matter is largely unknown, the simplest assumption which can explain all existing observations is that it is made of a new, yet undiscovered particle. Leading examples are Weakly Interacting Massive Particles (WIMPs), axions or axionlike-particles (ALPs) and sterile neutrinos. WIMPs with masses in the GeV range, as well as axions/ALPs are examples for Cold Dark Matter (CDM), while sterile neutrinos with masses at the keV-scale are an example for Warm Dark Matter (WDM). While CDM particles were non-relativistic at the time of their decoupling from the rest of the particles in the early universe, WDM particles remain relativistic for longer, retaining a larger velocity dispersion and more easily free-streaming out from small-scale perturbations. Astrophysical and cosmological observations constrain the mass of WDM to be larger than 3 keV/c^2, with a more recent lower limit from Lyman-α forest data being 5.3 keV.

A large number of experiments aim to observe axions/ALPs and WIMPs: directly, indirectly, or via production at the LHC. Direct detection experiments, which look for low energy nuclear recoils produced in collisions of WIMPs with atomic nuclei feature low energy thresholds, large detector masses and ultra-low backgrounds. Such experiments can thus also observe other type of particles, with non-vanishing couplings to electrons. Among these, bosonic super-WIMPs are an example for WDM. These particles, with masses at the keV-scale, could couple electromagnetically to Standard Model particles via the axio-electric effect, which is an analogous process to the photoelectric effect, and thus be detected in direct detection experiments.

This abstract is a review of experiments and studies about searching for vector and pseudoscalar bosonic super-WIMPs. It is organized as follows. Every experiment will have it's own chapter. The chapter will cover main facts and a short summary about the experiment in the first section, the second section will cover expected signals, rates and data analysis methods and etc. The third one will consist of existing results, findings and expectations.

1. LIGHT DARK MATTER CANDIDATES

In this chapter the dark matter candidate scenarios will be listed and shortly described. Also the interaction rates in a detector will be discussed.

1.1. PSEUDOSCALAR DM

The interactions can be wrote as a combination of several derivative-like operators of dimension five:

$$\mathcal{L}_{int} = \frac{C_\gamma a}{f_a} F_{\mu\nu}\widetilde{F}^{\mu\nu} - \frac{\partial_\mu a}{f_a}\bar{\psi}\gamma^\mu\gamma^5\psi + ... \quad , \tag{1.1}$$

where $F_{\mu\nu}$ and ψ are the electromagnetic field strength and the Dirac field of the electrons, and the ellipsis denotes possible interactions with other fermions and gauge bosons, and for simplicity we shall assume a similar strength for the a-SM couplings in those sectors. While the dimensionful coupling f_a does regulate the overall strength of the SM-a interaction, the dimensionless coupling to photons C_γ is crucial for determining the lifetime and γ-background created by a decay. Restricting to the electron-photon sector, three generic possibilities for the size of the coupling C_γ are expected:

$$\begin{aligned} A: &\qquad C_\gamma \sim \frac{\pi}{\alpha} \\ B: &\qquad C_\gamma \sim \frac{\alpha}{4\pi} \\ C: &\qquad C_\gamma \sim \frac{\alpha}{\pi} \times \frac{m_a^2}{m_e^2} \end{aligned} \tag{1.2}$$

Case A corresponds to a pseudoscalar coupled to photons at some UV normalization scale, with couplings to electrons generated radiatively. Having normalized the electron coupling to $1/f_a$ in 1.1, the coupling $C_\gamma \gg 1$ in

this case. Case C is the inverse of Case A. The derivative coupling to the electron axial-vector current may only lead to the $F_{\mu\nu}\widetilde{F}^{\mu\nu}\partial_\mu^2 a$ operator at loop level, hence the $(m_a/m_e)^2$ suppression. Finally, Case B is intermediate, when a is initially coupled to the fermion via the $m\psi i\gamma_5\psi$ pseudoscalar operator. Clearly any of these three choices can be realized without fine tuning given an appropriate UV completion. An additional advantage of this model is the automatic protection of the pseudoscalar mass 3 against radiative corrections, exactly as in the conventional axion case. As we are going to see later, only option C allows for the possibility of keV-scale dark matter without imposing overly strong constraints on the size of f_a.

1.2. VECTOR DM

A model of keV-scale vector dark matter can be introduced by choosing the initial Lagrangian in the form identical to that studied in [5], where an extra U(1)' gauge field is coupled to the SM via kinetic mixing with the hypercharge field strength,

$$\mathcal{L} = -\frac{1}{4}V_{\mu\nu}^2 - \frac{\kappa}{2}V_{\mu\nu}F_{\mu\nu} + \mathcal{L}_{h'} + \mathcal{L}_{dim>4} \quad , \tag{1.3}$$

with $\mathcal{L}_{h'}$ encoding the physics responsible for breaking the U(1)' , and $\mathcal{L}_{dim>4}$ includes possible non-renormalizable higher-dimension interaction terms. After the breaking of this secluded U(1)', the model takes the simplest possible form,

$$\mathcal{L} = -\frac{1}{4}V_{\mu\nu}^2 + \frac{1}{2}m_V^2 V_\mu^2 + \kappa V_{nu}\partial_\mu F_{\mu\nu} + ... \quad , \tag{1.4}$$

This is one of the simplest UV-complete extensions of the SM, and it has been addressed in connection with electroweak-scale physics on a number of occasions.

1.3. INTERACTION RATES IN A DETECTOR

Viable models for super-WIMPs as dark matter candidates result in vector and pseudo-scalar particles. The expected interaction rates in a detector

are obtained by convoluting the absorption cross section with the expected flux of these particles. The absorption cross section σ_{abs} for vector super-WIMPs can be written in terms of the cross section for photon absorption via the photoelectric effect σ_{pe}, with the photon energy ω replaced by the mass of the vector boson m_v:

$$\frac{\sigma_{abs} v}{\sigma_{pe}(\omega = m_v)c} \approx \frac{\alpha'}{\alpha}, \tag{1.5}$$

where v is the incoming velocity of the vector boson, c is the velocity of light, α and α' are the fine structure constant, and its vector boson equivalent, respectively. For pseudo-scalar super-WIMPs, the relation between the two cross sections is as follows:

$$\frac{\sigma_{abs} v}{\sigma_{pe}(\omega = m_a)c} \approx \frac{3m_a^2}{4\pi\alpha f_a^2}, \tag{1.6}$$

where m_a is the mass of the pseudo-scalar particle, and f_a is a dimensional coupling constant.

Assuming that super-WIMPs are non-relativistic, and that their local density is 0.3 GeV/cm^3, the interaction rate in a direct detection experiment can be expressed using equations 1.5 and 1.6 as [6]:

$$R \sim \frac{4 \times 10^{23}}{A} \frac{\alpha'}{\alpha} \left(\frac{keV}{m_v}\right) \left(\frac{\sigma_{pe}}{b}\right) kg^{-1} d^{-1}, \tag{1.7}$$

and

$$R \sim \frac{1.29 \times 10^{19}}{A} g_{ae}^2 \left(\frac{m_a}{keV}\right) \left(\frac{\sigma_{pe}}{b}\right) kg^{-1} d^{-1}, \tag{1.8}$$

for vector and pseudo-scalar super-WIMPs, respectively. $g_{ae} = 2m_e f_a^{-1}$ is the axio-electric coupling, m_e is the mass of the electron, and A is the atomic number of the target atom.

2. XENON100 DETECTOR

2.1. EXPERIMENT REVIEW

Located at the Laboratori Nazionali del Gran Sasso (LNGS), the XENON100 experiment operates a dualphase (liquid and gas) xenon time projection chamber (TPC). The detector contains 161 kg of LXe in total, with 62 kg in the active region of the TPC. A total of 178 1-inch square, low-radioactivity, UV-sensitive photomultiplier tubes (PMTs) arranged in two arrays, one in the liquid and one in the gas, detect the prompt scintillation (S1) and the delayed, proportional scintillation signal (S2) arising when a particle interacts in the TPC.

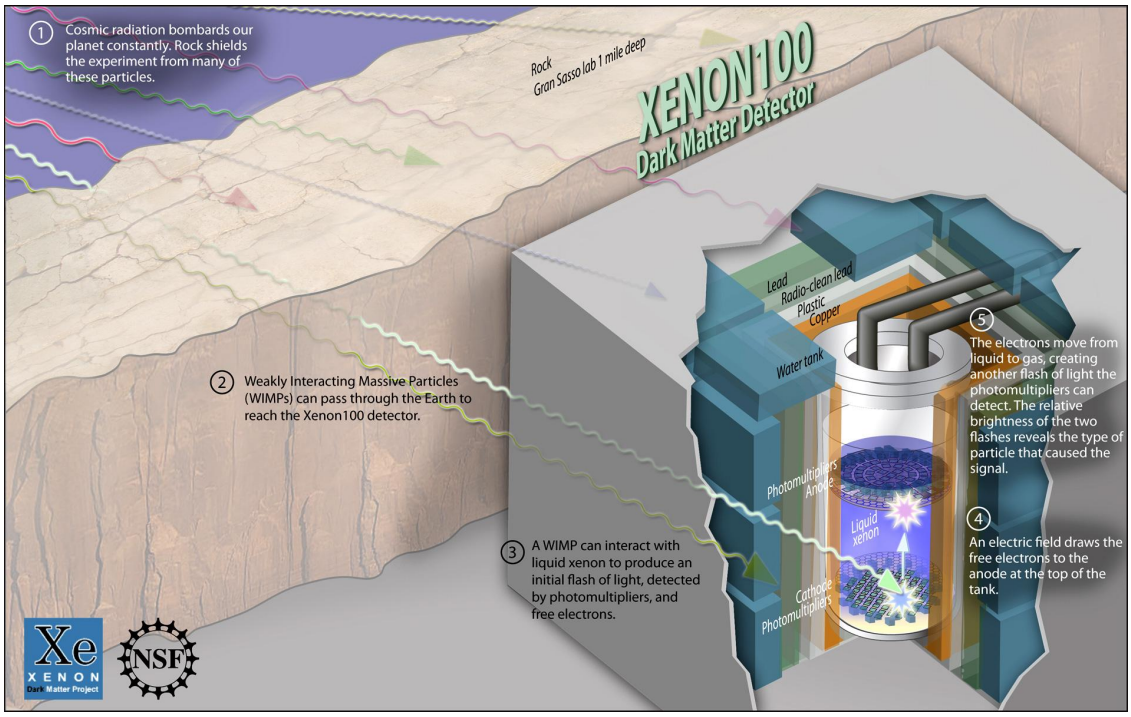

Figure 2.1 — XENON100 operational principles

The ionisation electrons are drifted via an electric field of 530 V/cm to the liquid-gas boundary and extracted in the vapour phase via a 12 kV/cm field, where proportional scintillation is produced. The three-dimensional position of the original interaction site is reconstructed via the time difference between the S1 and S2 signal (z-position, with a 1 σ resolution $<$0.3 mm), and by

exploiting the S2 light pattern in the top PMT array ((x, y)-position, with a 1 σ resolution <3 mm). This enables us to reject a large fraction of background events via fiducial volume cuts and selection of single-scatters. A 4 cm thick, 99 kg LXe, layer surrounds the TPC and is observed by 64 1-inch square PMTs, allowing us to rejects events with energy depositions in this active LXe region. Finally, nuclear recoils (NRs) induced by fast neutrons and WIMPnucleus scatters, and electronic recoils (ERs), produced by β and γ-rays, as well as axions, can be distinguished based on their (S2/S1)-ratio. The XENON100 experiment, has delivered competitive constraints on spinindependent and spin-dependent WIMP-nucleus scatters, on solar axions and galactic ALPs, as well as on leptophilic dark matter models.

2.2. EXPECTED SIGNAL AND ANALYSIS

With equations (1.7) and (1.8), we can predict the interaction rate in XENON100, assuming a range of coupling constants, and an exposure of 34 kg$\times$224.6 live days, as shown in figures 2.2 and 2.3 for vector and pseudo-scalar super-WIMPs, respectively. The structures observed around 35 keV, as well as at lower energies are due to an increase in the cross section of the photoelectric effect in xenon at these energies, when new atomic energy levels are excited.

Analysis was performed using XENON100 Run II science data, with 224.6 live days of data and 34 kg of LXe in the fiducial region. The overall background in the low-energy region is 5.3×10^{-3} events/(kg d keV) and it is flat in shape, because it is dominated by Compton scatters of high-energy gammas originating from the radio-activity of detector materials.

An interaction in the LXe-TPC gives rise to an S1 and a correlated S2 signal with a certain number of photoelectrons (PE) observed by the photosensors. Selection criteria is described in [7]. These include basic data quality selection criteria, single-scatter and fiducial volume selection, and signal consistency checks.

The combined acceptance of all applied event selection criteria, evaluated on calibration data acquired with ^{60}Co and ^{232}Th sources, is shown in figure 2.4.

The background events in the region of interest are predominantly due

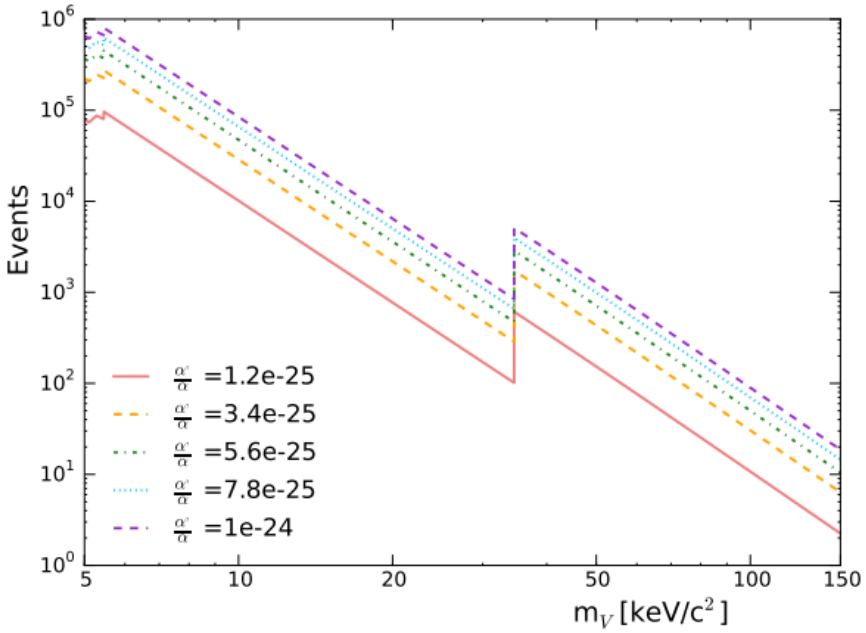

Figure 2.2 — Predicted total number of events, assuming an infinite energy resolution, for vector super-WIMPs in XENON100 as a function of mass for a range of coupling constants. The assumed exposure is 34 kg×225 live days of data.

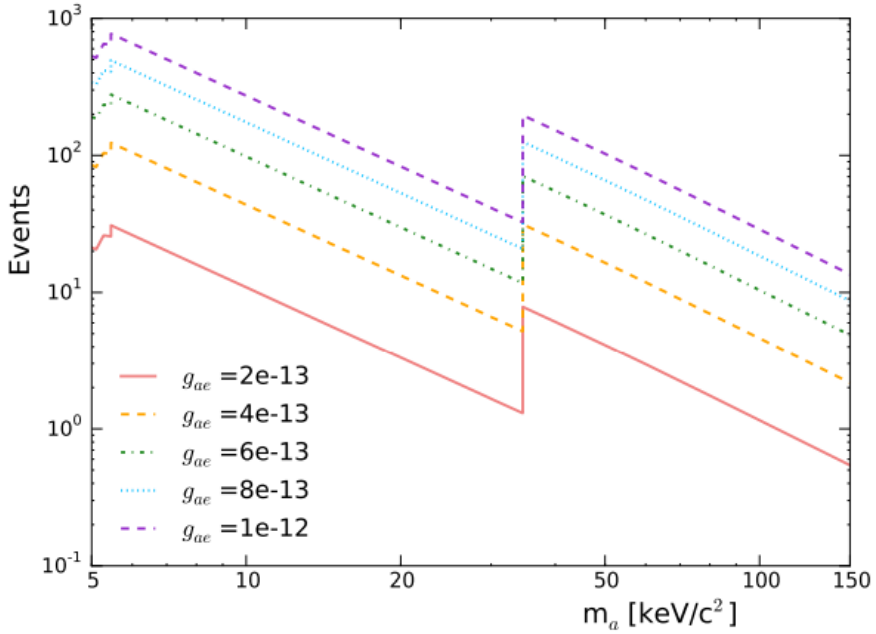

Figure 2.3 — Predicted total number of events, assuming an infinite energy resolution, for pseudo-scalar super-WIMPs in XENON100 as a function of mass for a range of coupling constants. The assumed exposure is 34 kg×225 live days of data.

to interactions of γ-rays from decays of radioactive isotopes in the detector

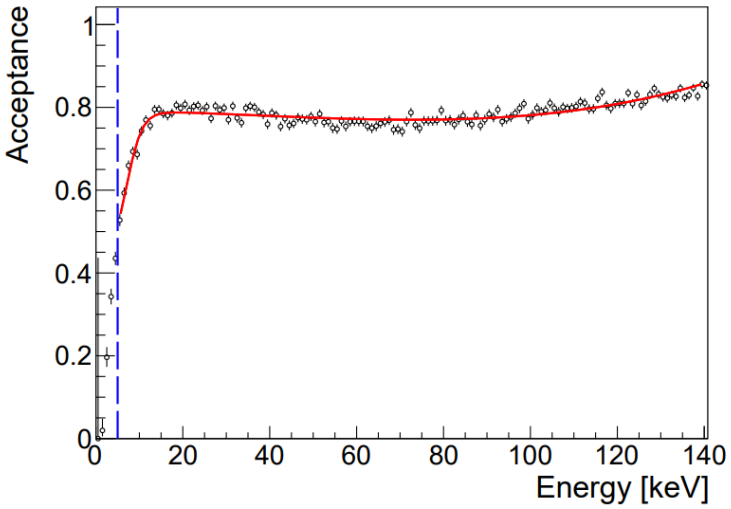

Figure 2.4 — Calculated acceptance ϵ (black dots) of all the event selection criteria as a function of energy, along with a fit (red curve) to the distribution. The energy threshold employed in the analysis (5 keV) is shown by the vertical dashed line.

materials, yielding low-energy Compton-scatters, and from β-decays of the ^{222}Rn and ^{85}Kr isotopes distributed in the liquid xenon. To model the expected shape of the background distribution in the region of interest, authors of [8] employ calibration data acquired with ^{60}Co and ^{232}Th sources. The spectral shape is parameterised with a modified Fermi function, as shown in figure 2.5, together with the calibration data.

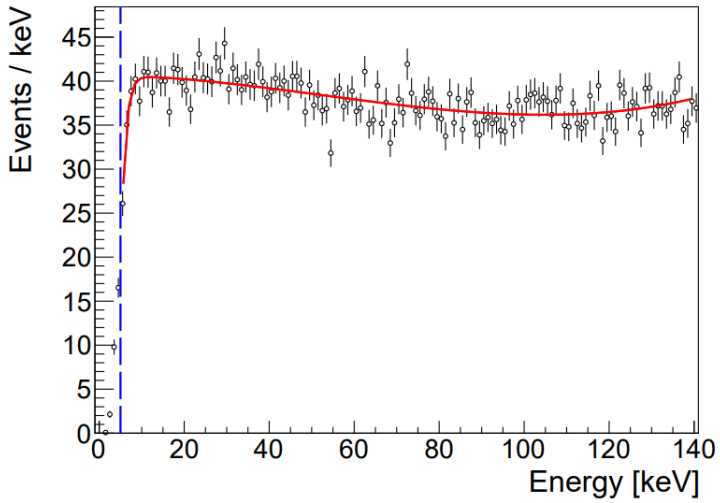

Figure 2.5 — Background model (red line) scaled to the correct exposure. The model is based on ^{60}Co and ^{232}Th calibration data (black dots). The energy threshold of 5 keV is shown by the vertical dashed line.

For each considered mass m_a of the bosonic superWIMP, the $\pm 2 - \sigma$-

region, as determined by the energy resolution at the given energy, is blinded. The number of events outside of this region is then used to scale the background model shown in figure 2.5, and thus to predict the number of expected background events in the signal region. Since the $\pm 2 - \sigma$ window must not exceed the search region between (5-140) keV, the range of bosonic super-WIMP masses is restricted to (8-125) keV.

2.3. RESULTS

Figure 2.6 shows the distribution of events in the region of interest, together with the expected signal for different pseudo-scalar super-WIMP masses and an assumed coupling of $g_{ae} = 1 \times 10^{-12}$

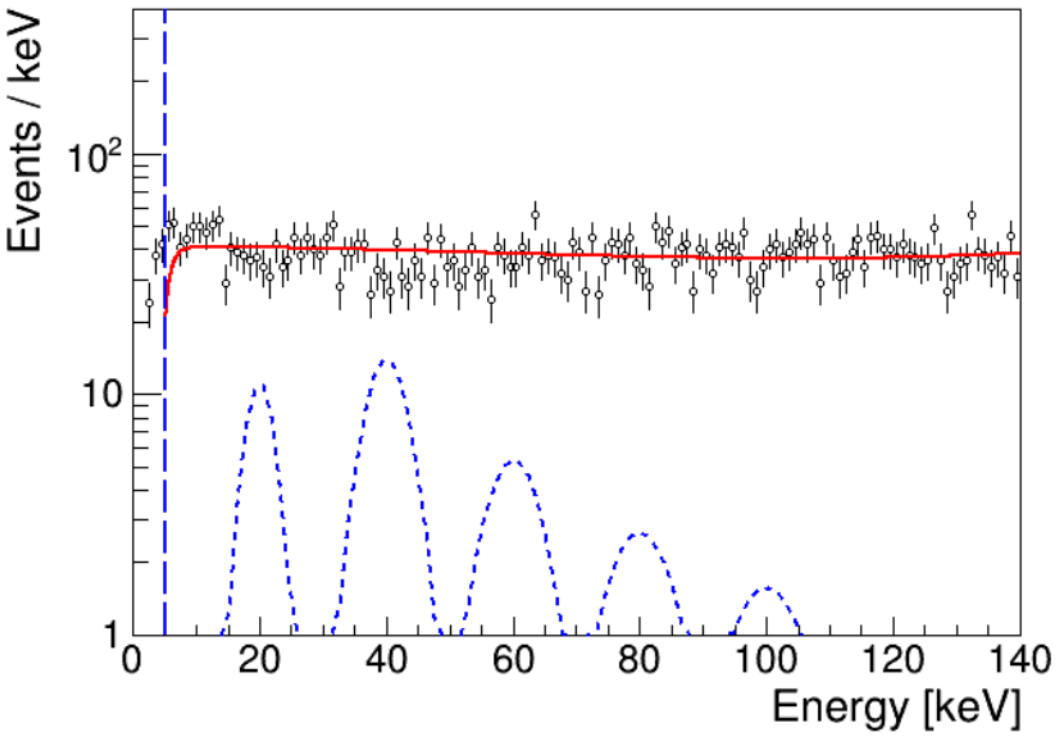

Figure 2.6 — Distribution of events (black dots with error bars) in the super-WIMP search region between (5 - 140) keV. The background model (red curve) along with the expected signal for various pseudo-scalar super-WIMP masses (20, 40, 60, 80 and 100 keV) and a coupling of $g_{ae} = 1 \times 10^{-12}$ (blue dashed peaks) is also shown. The vertical dashed line indicated the energy threshold in this analysis.

Figure 6 shows the 90% C.L. exclusion limit for pseudoscalar (top panel)

and vector (bottom panel) superWIMPs. The step in sensitivity around 35 keV/c^2 is due to an increase in the photoelectric cross section as new atomic energy levels are excited.

The observed fluctuations in the limit are caused by statistical fluctuations in the background (see figure 2.6). Due to the expected mono-energetic shape of the signal, the limit is very sensitive to such fluctuations. Authors of [8] have also studied the impact of systematic uncertainties on the analysis. In particular, they have considered the impact of varying the overall event selection acceptance, the energy resolution, as well as the energy scale.

The combined effect of all systematic uncertainties changes the final result by around 10%, however this contribution is small compared to the statistical uncertainty that is accounted for in the profile likelihood analysis. XENON100 thus sets new and stringent upper limits in the (8 - 125) keV/c^2 mass range. At 90% C.L. it excludes couplings to electrons $g_{ae} > 3 \times 10^{-13}$ for pseudoscalar super-WIMPs and $\alpha'/\alpha > 2 \times 10^{-28}$ for vectorsuper-WIMPs. These limits are derived under the assumption that super-WIMPs constitute all of the galactic dark matter.

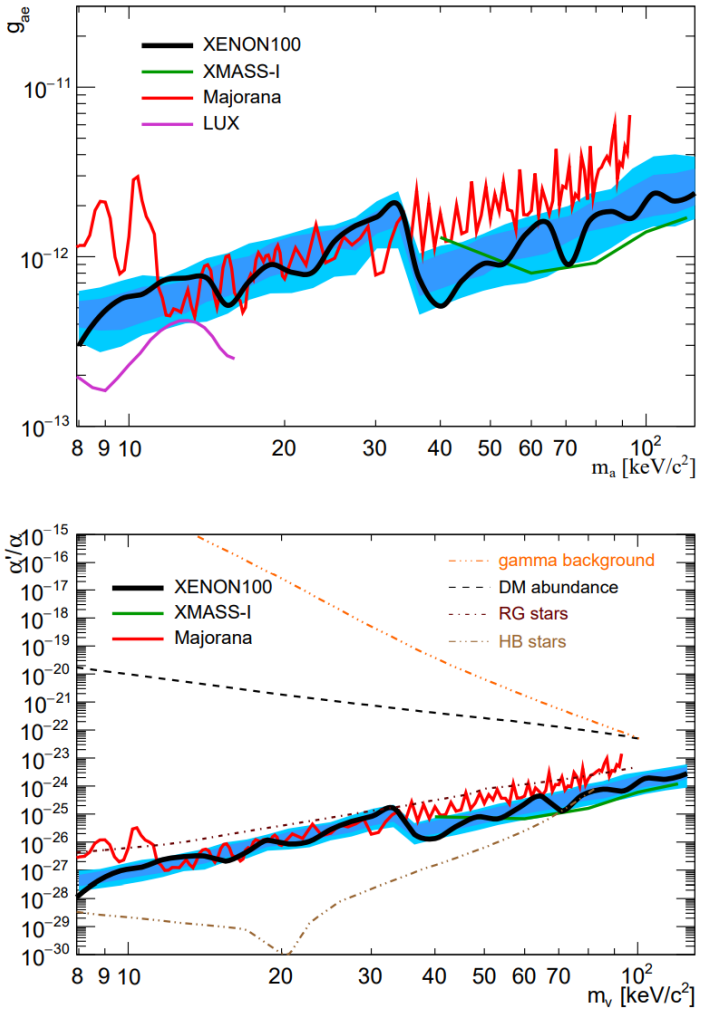

Figure 2.7 — The XENON100 upper limits, at 90% C.L., on the coupling of pseudo-scalar (top) and vector (bottom) superWIMPs as a function of particle mass. The 1-σ (2-σ) expected sensitivity is shown by the dark (light) blue bands. The limits are compared to the results obtained by the XMASS-I [9] (green), LUX [10] (magenta) and Majorana Demonstrator [11] (red) experiments, as well as with astrophysical constraints from the gamma background, the dark matter abundance, red giant stars and horizontal branch stars (dashed and dashdotted) [6] for the case of the vector super-WIMP.

3. XMASS-I DETECTOR

3.1. EXPERIMENT REVIEW

XMASS-I is a large single phase liquid-xenon detector located underground (2700 m water equivalent) at the Kamioka Observatory in Japan. An active target of 835 kg of liquid xenon is held inside of a pentakis-dodecahedral copper structure that holds 642 inwardlooking photomultiplier tubes (PMTs) on its approximately spherical inner surface. The detector is calibrated regularly by inserting ^{57}Co and ^{241}Am sources along the central vertical axis of the detector. Measuring with the 57Co source from the center of the detector volume the photoelectron yield is determined to be 13.9 photoelectrons (p.e.)/keV$_{ee}$, where the subscript ee refers to the customary electron equivalent energy deposit.

This large photoelectron yield is realized since the photocathode area covers >62% of the inner wall with large quantum efficiency of $\sim$ 30%. Data acquisition is triggered if ten or more PMTs have signals larger than 0.2 p.e. within 200 ns. Each PMT signal is digitized with charge and timing resolution of 0.05 p.e. and 0.4 ns, respectively. The liquid-xenon detector is located at the center of a water Cherenkov veto counter, which is 11 m high and has 10 m diameter. The veto counter is equipped with 72 50 cm PMTs. Data acquisition for the veto counter is triggered if eight or more of its PMTs register a signal within 200 ns. XMASS-I is the first direct detection dark matter experiment equipped with such an active water Cherenkov shield.

3.2. EXPECTED SIGNAL AND ANALYSIS

This chapter is based mostly on study [9] which use Monte Carlo simulations to increase event selection efficiency. For both, vector and pseudoscalar type super-WIMPs, Monte Carlo (MC) signals are generated by injecting gamma rays uniformly over the entire active volume with a gamma energy corresponding

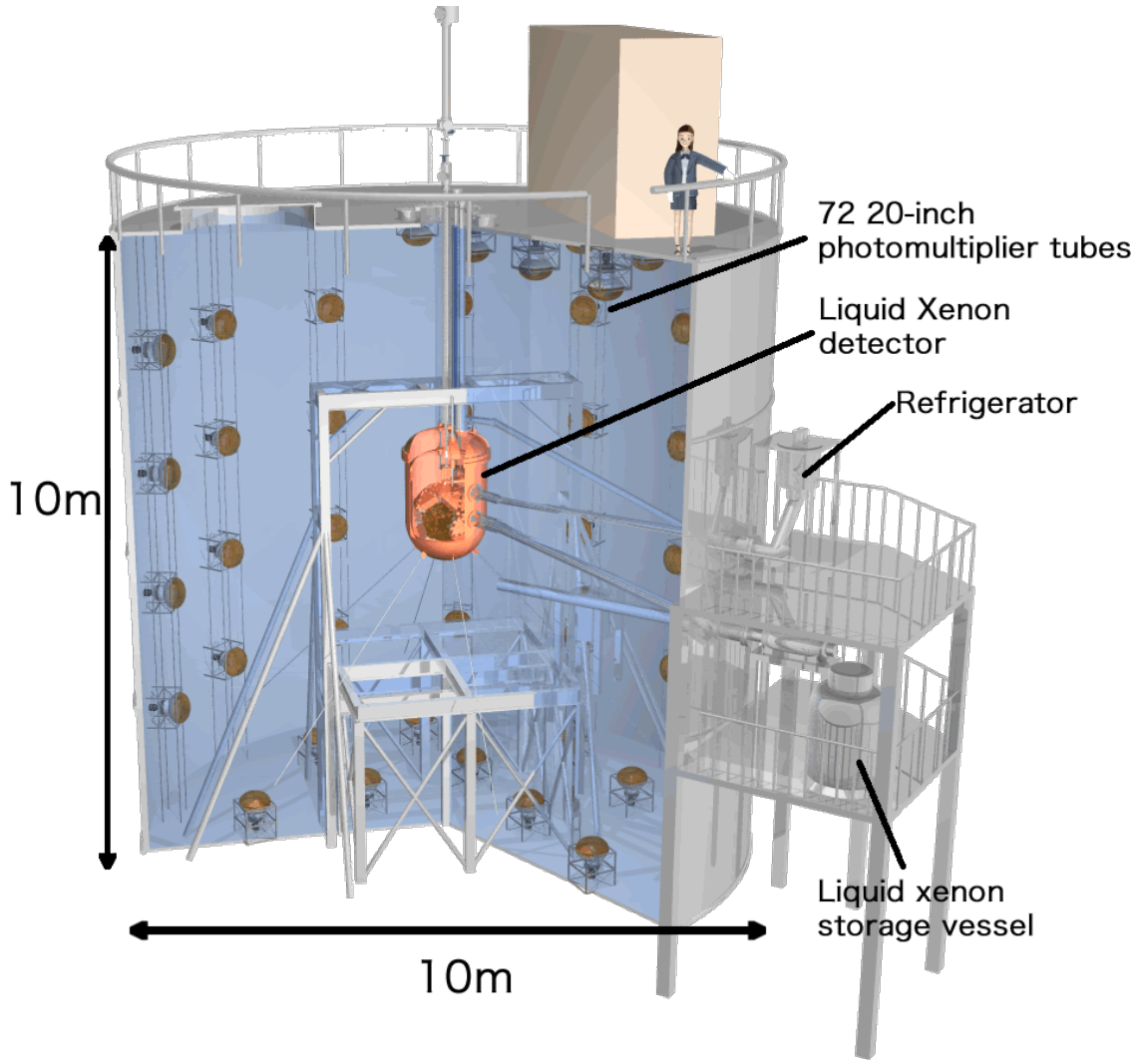

Figure 3.1 — Overview of XMASS detector

to the rest mass of the boson. This procedure exploits the experimentally relevant aspect that all the energy of a boson including its mass given to an electron is identical to that for gamma rays at these low energies, albeit with different coupling constants in Eqs. (1.7) and (1.8), listed in a previous chapter.

Data taken in the commission phase between December 24, 2010 and May 10, 2012 were used for the analysis in [9]. Authors selected the periods of operation under what they designate normal data taking conditions with a stable temperature (174±1.2 K) and pressure (0.160- 0.164 MPa absolute). They have further removed the periods of operation with excessive PMT noise, unstable pedestal levels, or abnormal trigger rates. Total livetime is 165.9 days. Event selection proceeds in four stages that we refer to as cut-1 through cut-4. Cut-1 requires that no outer detector trigger is associated with the events, that they are separated from the nearest event in time by at least 10 ms, and that

the RMS spread of the inner detector hit timings contributing to the trigger is less than 100 ns. These criteria eliminate events that are electronics or detector artifacts rather than physical interactions in the detector. Their application reduces the total effective lifetime to 132.0 days in the final sample.

The main source of background to the physics analyses stems from surface background, especially the radioactive contaminants in the aluminum seal of the PMTs. Authors of [9] used three additional cuts to reduce those backgrounds. Cut-2 makes use of an event vertex reconstruction. This reconstruction is based on a maximum likelihood evaluation of the observed light distribution in the detector.

The remaining two cuts deal with the issue of mis-reconstructed events. In particular radioactive decays on the inner surfaces of the detector pose a problem since light emitted from the flat areas between the PMTs is not necessarily detected by those PMTs surrounding the emission point. Two cuts were developed to identify and eliminate such events. Cut-3 uses the time difference δT_m between the first hit in an event and the mean of the timings of the second half of all the time-ordered hits in the event. Events with smaller δT_m are less likely to be mis-reconstructed surface events and are kept. Cut-4 eliminates events that reflect their origin within groves or crevices in the inner detector surface through a particular illumination pattern. Figure 3.2 shows the distributions of the cut variables described above for 57Co source data and the respective simulations. The reasonable agreement demonstrates the validity of the simulation.

To maximize the sensitivity, cut values are optimized for each super-WIMP mass using its respective super-WIMP MC simulation. The optimization was done by maximizing the ratio of the number of expected signal events to the number of observed background events just outside the signal range.

Figure 3.3 shows data and simulated signal after applying all the cuts.

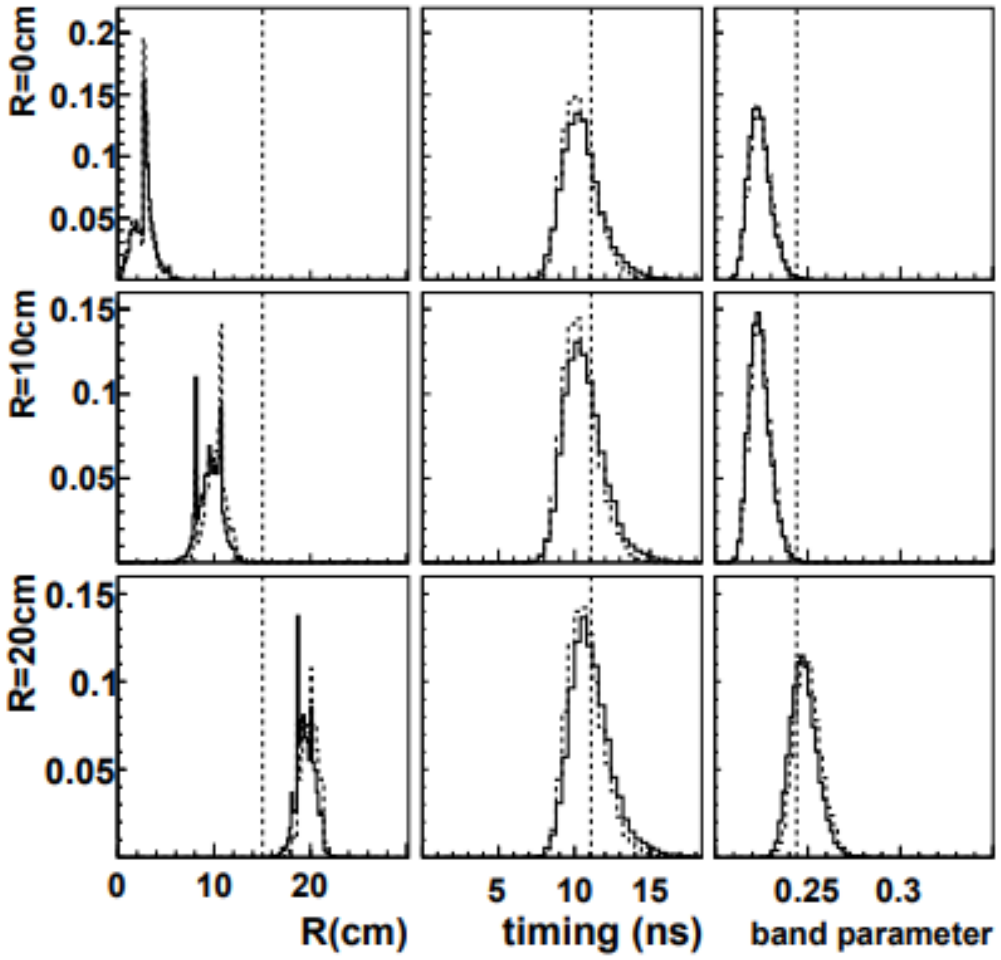

Figure 3.2 — Comparisons of 122 keV gamma ray data (solid histograms) with simulation (dashed histograms) at three positions in the detector, R = 0 cm, 10 cm, and 20 cm, from the top to bottom rows. From left to right, distributions for R, δT_m, and F_B are shown. Data and simulation are in reasonable agreement. The vertical dashed lines show the cut values for 120 keV.

3.3. RESULTS

Upper limit on the coupling constants for assumed masses, as well as chosen cut parameters given in table 3.4. Optimized cuts for several cases of m_b. Columns R, δT_m, and F_B list the chosen cut values. Column E shows the range of the signal window in keV_{ee}. Signal efficiencies are obtained from the detector simulation, by taking the ratio between the number of events in the hatched histogram in Fig. 3.3 and the number of events generated in the fiducial mass, 41 kg, inside the radius 15 cm of the detector. The number of observed events within the signal window is listed in the "obs."column. The last two

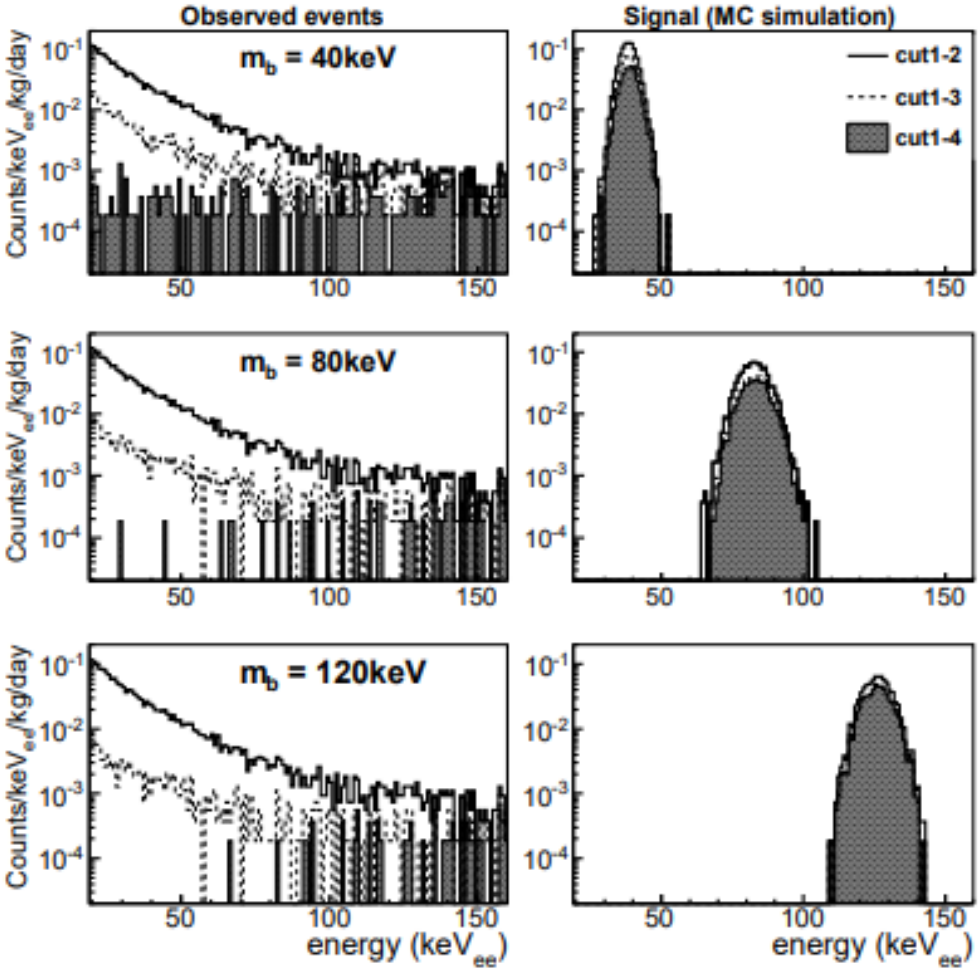

Figure 3.3 — Energy distribution of the observed events (left column) and simulated events (right column) remaining after each step of the cuts optimized for each vector boson mass individually. From top to bottom, m_b =40, 80, and 120 keV, respectively. In each figure, three histograms are showing events after the cumulative cuts 1-2 (dotted line), cuts 1-3 (dashed line), and cut 1-4 (hatched histogram). The effective livetime is 132.0 days and the target mass is 41 kg. The small number of events at the low energy region in the final samples are due to lower efficiency of cut-4.

columns show the resulting constraints on α'/α and g_{aee} at 90% CL.

Resulting constraints on α'/α and g_{aee} are also shown in figure 3.5

This is the first direct search for vector bosonic super-WIMPs in this mass range. In this range the present result excludes the possibility for such WIMPs to constitute all of dark matter. As can be seen in the figure, the obtained limit also is comparable to or better than the current astrophysical constraints. For pseudoscalar superWIMPs coupling the present limit improves significantly on previous results [12] [7]. This significant improvement was achieved exploiting

m_b (keV)	R (cm)	δT_m (ns)	F_B	E (keV$_{ee}$)	eff. (%)	obs.	^{214}Pb expected	α'/α	g_{aee}
40	<15	<12.62	<0.258	23.7–53.7	51±13	48	7.9 ± 0.7	8.0×10^{-26}	1.3×10^{-12}
60	<15	<12.54	<0.248	46.9–76.9	63±16	12	11.6 ± 1.0	6.8×10^{-26}	8.0×10^{-13}
80	<15	<11.51	<0.246	68.1–98.1	59±18	8	9.6 ± 0.8	1.6×10^{-25}	9.2×10^{-13}
100	<15	<11.14	<0.244	89–119	65±20	15	11.4 ± 1.0	6.0×10^{-25}	1.4×10^{-12}
120	<15	<11.11	<0.244	111–141	74±23	18	14.4 ± 1.1	1.2×10^{-24}	1.7×10^{-12}

Figure 3.4 — Achieved constraints α'/α and g_{aee} at 90% CL and cut parameters for m_b 40, 60, 80, 100 and 120 keV

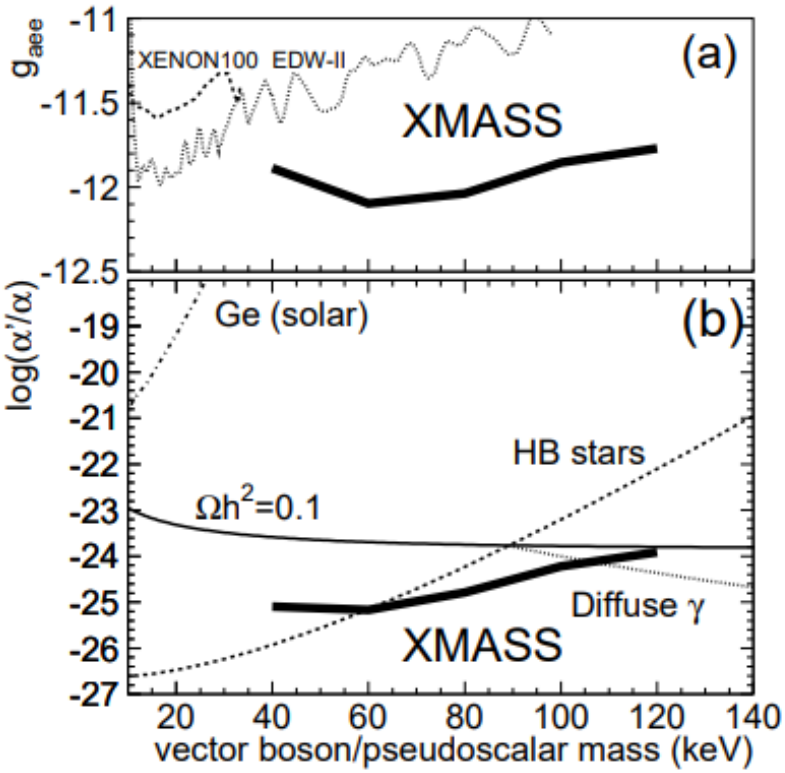

Figure 3.5 — Limits on coupling constants for (a) electrons and pseudoscalar bosons and (b) electrons and vector bosons at 90% CL (thick solid line). (a) Dashed line and dotted line correspond to constraints obtained by EDELWEISS-II [12] and XENON100 [7]. (b) The thin solid line corresponds to the coupling constant required to reproduce the observed dark matter abundance including resonance effects. The dotted line and dashed line correspond to the upper limit from the γ-ray background from 3γ decays in the Galaxy, and the constraint from the He-burning lifetime in horizontal branch (HB) stars. The dash-dotted line shows an experimental constraint assuming production in the Sun.

the low background in the detector, unprecedented in this energy range.

In summary, in 165.9 days of data with an effective livetime of 132.0 days in a fiducial mass of 41 kg, no significant signal was observed and stringent limits on the electron coupling of bosonic super-WIMPs with masses in the 40-120 keV range were obtained. For vector bosons the present experimental limit excludes the possibility that vector super-WIMPs constitute all the dark matter. The absence of the signal also provides the most stringent direct constraint on the coupling constant of pseudoscalar dark matter to electrons.

REFERENCES

1. Planck 2013 results. XVI. Cosmological parameters / Planck Collaboration [et al.] // A&A. — 2014. — Vol. 571. — A16.
2. *Kaiser N.*, *Squires G.* Mapping the Dark Matter with Weak Gravitational Lensing // apj. — 1993. — Vol. 404. — P. 441.
3. *Rubin V. C.*, *Ford W. Kent J.* Rotation of the Andromeda Nebula from a Spectroscopic Survey of Emission Regions // apj. — 1970. — Vol. 159. — P. 379.
4. *Frenk C.*, *White S.* Dark matter and cosmic structure // Annalen der Physik. — 2012. — Vol. 524, no. 9/10. — P. 507–534. — eprint: https://onlinelibrary.wiley.com/doi/pdf/10.1002/andp.201200212.
5. *Pospelov M.*, *Ritz A.*, *Voloshin M.* Secluded WIMP dark matter // Physics Letters B. — 2008. — Vol. 662, no. 1. — P. 53–61. — ISSN 0370-2693.
6. *Pospelov M.*, *Ritz A.*, *Voloshin M.* Bosonic super-WIMPs as keV-scale dark matter // Phys. Rev. D. — 2008. — Vol. 78, issue 11. — P. 115012.
7. First axion results from the XENON100 experiment / E. Aprile [et al.] // Phys. Rev. D. — 2014. — Vol. 90, issue 6. — P. 062009.
8. Search for bosonic super-WIMP interactions with the XENON100 experiment / E. Aprile [et al.] // Physical Review D. — 2017. — Vol. 96, no. 12. — ISSN 2470-0029.
9. Search for Bosonic Superweakly Interacting Massive Dark Matter Particles with the XMASS-I Detector / K. Abe [et al.] // Physical Review Letters. — 2014. — Vol. 113, no. 12. — ISSN 1079-7114.

10. First Searches for Axions and Axionlike Particles with the LUX Experiment / D. S. Akerib [et al.] // Physical Review Letters. — 2017. — Vol. 118, no. 26. — ISSN 1079-7114.

11. New Limits on Bosonic Dark Matter, Solar Axions, Pauli Exclusion Principle Violation, and Electron Decay from the Majorana Demonstrator / N. Abgrall [et al.] // Phys. Rev. Lett. — 2017. — Vol. 118, issue 16. — P. 161801.

12. Axion searches with the EDELWEISS-II experiment / E. Armengaud [et al.] // Journal of Cosmology and Astroparticle Physics. — 2013. — Vol. 2013, no. 11. — P. 067–067. — ISSN 1475-7516.